Structural Diversity of Solid Dispersions of Acetylsalicylic Acid As Seen by Solid-State NMR

ARTICLE *in* MOLECULAR PHARMACEUTICS · JANUARY 2014

Impact Factor: 4.38 · DOI: 10.1021/mp400495h · Source: PubMed

molecular pharmaceutics

Article

pubs.acs.org/molecularpharmaceutics

Structural Diversity of Solid Dispersions of Acetylsalicylic Acid As Seen by Solid-State NMR

Olivia Policianova, Jiri Brus,* Martin Hruby, Martina Urbanova, Alexander Zhigunov, Jana Kredatusova, and Libor Kobera

Institute of Macromolecular Chemistry, Academy of Sciences of the Czech Republic, Heyrovského nám. 2, 162 06 Praha 6, Czech Republic

Supporting Information

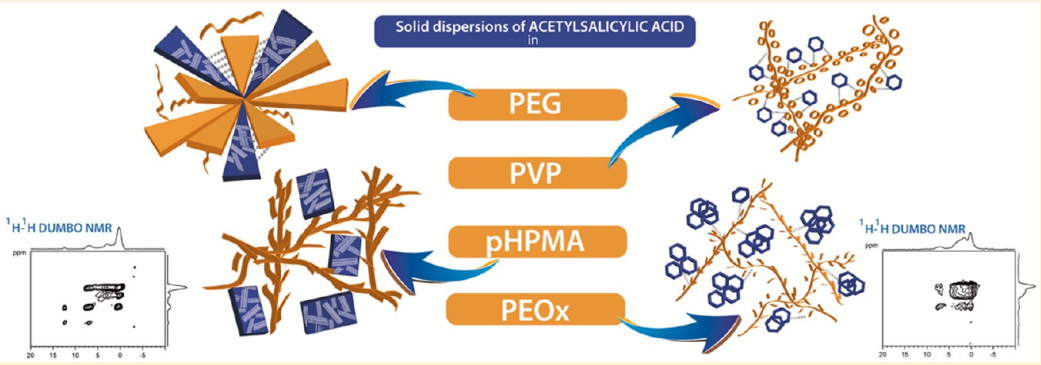

ABSTRACT: Solid dispersions of active pharmaceutical ingredients are of increasing interest due to their versatile use. In the present study polyvinylpyrrolidone (PVP), poly[*N*-(2-hydroxypropyl)-metacrylamide] (pHPMA), poly(2-ethyl-2-oxazoline) (PEOx), and polyethylene glycol (PEG), each in three M_w, were used to demonstrate structural diversity of solid dispersions. Acetylsalicylic acid (ASA) was used as a model drug. Four distinct types of the solid dispersions of ASA were created using a freeze-drying method: (i) crystalline solid dispersions containing nanocrystalline ASA in a crystalline PEG matrix; (ii) amorphous glass suspensions with large ASA crystallites embedded in amorphous pHPMA; (iii) solid solutions with molecularly dispersed ASA in rigid amorphous PVP; and (iv) nanoheterogeneous solid solutions/suspensions containing nanosized ASA clusters dispersed in a semiflexible matrix of PEOx. The obtained structural data confirmed that the type of solid dispersion can be primarily controlled by the chemical constitutions of the applied polymers, while the molecular weight of the polymers had no detectable impact. The molecular structure of the prepared dispersions was characterized using solid-state NMR, wide-angle X-ray scattering (WAXS), and differential scanning calorimetry (DSC). By applying various ^{1}H−^{13}C and ^{1}H−^{1}H correlation experiments combined with $T_1(^1\mathrm{H})$ and $T_{1\rho}(^1\mathrm{H})$ relaxation data, the extent of the molecular mixing was determined over a wide range of distances, from intimate intermolecular contacts (0.1−0.5 nm) up to the phase-separated nanodomains reaching ca. 500 nm. Hydrogen-bond interactions between ASA and polymers were probed by the analysis of ^{13}C and ^{15}N CP/MAS NMR spectra combined with the measurements of ^{1}H−^{15}N dipolar profiles. Overall potentialities and limitations of individual experimental techniques were thoroughly evaluated.

KEYWORDS: *solid dispersions, acetylsalicylic acid, polymers, solid-state NMR, structure, dynamics*

INTRODUCTION

The use of solid dispersions (SDs) to enhance the absorption of poorly water-soluble drugs was first proposed more than 40 years ago.[1] This concept is based on dispersing a hydrophobic active pharmaceutical ingredient (API) into a hydrophilic nontoxic matrix, such as polymers, glycerides, cellulose, or urea.[1−3] SDs are also important during early stage drug development because they maximize drug exposure during animal experimentation, facilitating the identification of toxicological effects. Moreover, solid dispersions can slow the dissolution rate of highly soluble drugs, generating thus promising controlled-drug-release systems. Despite extensive research in this field, applications of pharmaceutical solid dispersions have remained limited, and only a few products have been marketed thus far. This follows from the fact that SDs require laborious preparation methods, sometimes display irreproducible physicochemical characteristics, and exhibit problems during the scale-up manufacturing processes. Moreover their reliable structural characterization is extremely demanding.

Received: August 19, 2013
Revised: November 28, 2013
Accepted: January 13, 2014
Published: January 13, 2014

As demonstrated in Figure 1, a range of different types of solid dispersions can be distinguished. Formation of each

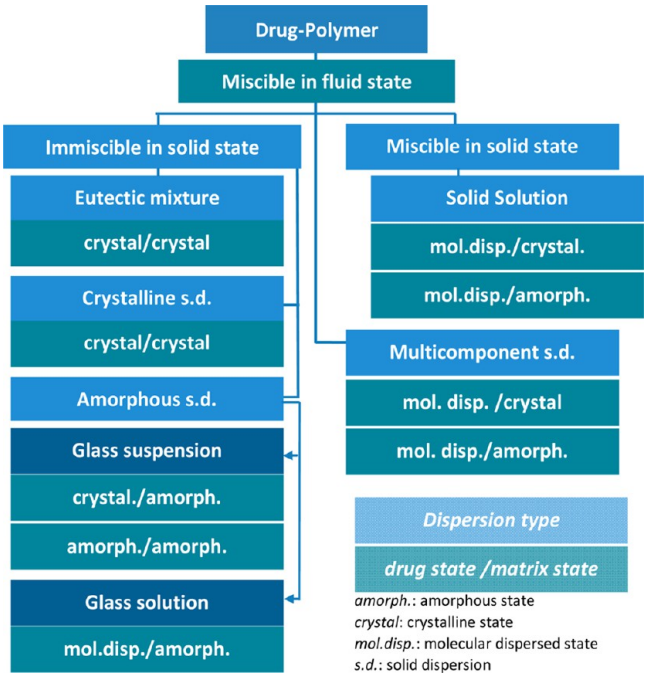

Figure 1. Schematic illustration of the classification of solid dispersions based on the state of their individual components.[4−6]

system depends on numerous factors, such as the miscibility of the individual components in their fluid state, the rates of solidification and crystallization of the individual components, and the synthetic procedure (e.g., freeze-drying, vacuum drying, spray drying, etc.). Similarly, the chemical constitution and molecular weight (M_w) of the applied polymers may affect not only the type of SDs but also their physicochemical properties, including wettability and stability during final storage.[4−10] Many studies have focused on polyethylene glycol (PEG) and polyvinylpyrrolidone (PVP), resulting in commercial products, such as Gris-PEG (griseofulvin in PEG), Sporanox (itraconazole in PEG), and Cesamet (nabilone in PVP).[11]

In contrast, other biocompatible water-soluble polymers, such as poly[*N*-(2-hydroxypropyl)-metacrylamide] (pHPMA) and poly(2-ethyl-2-oxazoline) PEOx, have rarely been tested in solid dispersions, despite their high potential for generating efficient drug delivery systems.[12−14] Literature search also shows that majority of current studies deals with enhancement of kinetic solubility of APIs from the Class II and IV of Biopharmaceutics Classification System (BCS) despite the fact that the decrease of solubility of APIs from the Class I can be in many aspects useful. The successful development and application of pharmaceutical SDs also require precise structural and physicochemical characterization because any structural deviation from the expected architecture may induce undesired changes in physicochemical properties. Therefore, studying polymer−drug interactions in solid dispersions and relating the chemical composition, 3D architecture, and physicochemical properties to one another is a fundamental and challenging step in the development of these pharmaceutical solids.

For our structural study we have chosen two nontraditional biocompatible water-soluble polymers (pHPMA and PEOx) and compared them with the commonly used PEG and PVP. Polymer pHPMA is known as a base of the copolymer systems used for passive drug targeting purposes in specific cancer therapy,[12,13] and PEOx is a useful base of copolymer micelles encapsulating hydrophobic drugs.[14] As an active compound we used acetylsalicylic acid (ASA), a drug with many positive clinical effects[15−17] recently reclassified into BCS Class I.[18,19] Moreover, ASA is a compound that cannot simply exist in an amorphous state. Because of the low T_g that is estimated to be ca. −30 °C, amorphization of ASA requires support by noncovalent bonding with excipients. ASA thus represents a suitable model system on which these interactions can be directly studied and the role of chemical nature of polymeric excipients can be evaluated.

The primary purpose of the presented investigation was to demonstrate that the 3D architecture of solid dispersions of APIs can be controlled by the chemical nature of polymer excipients. For this purpose we prepared by a freeze-drying method a set of solid dispersions of ASA. As a polymer matrix we used PEG, PVP, pHPMA, and PEOx, each of them in three different molecular weights. The secondary purpose of our study was to formulate an experimental protocol allowing comprehensive and reliable structural characterization of solid dispersions with different 3D architectures, including assessment of their homogeneity from the subnanometer scale up to the domains with the several hundred nanometers size.

MATERIALS AND METHODS

ASA (Sigma-Aldrich, St. Louis, USA), water-soluble biocompatible polymers (PVP, PEG, PEOx, and pHPMA), water, and *tert*-butanol (*t*-but) (Sigma-Aldrich, St. Louis, USA) were used to prepare solid dispersions (Chart 1). Polyethylene glycol ($PEG_{2000,6000,10000}$) and polyvinylpyrrolidone

Chart 1. Chemical Structures of the Applied Components: The Active Pharmaceutical Ingredient (ASA) and the Polymers (PVP, PEOx, pHPMA, and PEG)

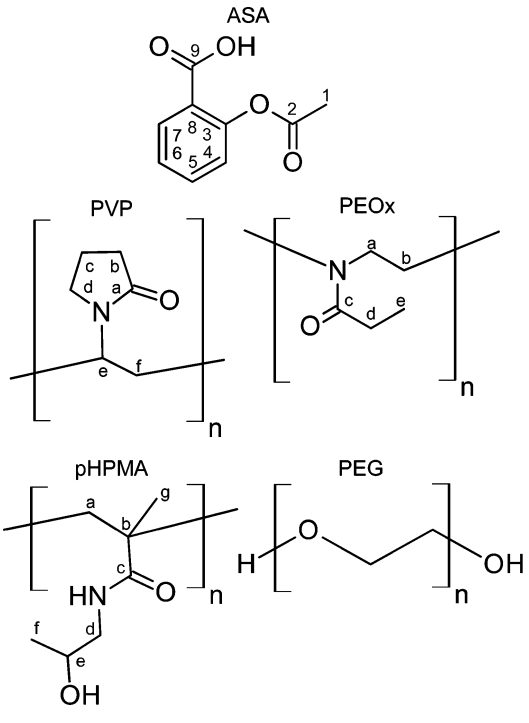

dx.doi.org/10.1021/mp400495h | *Mol. Pharmaceutics* 2014, 11, 516−530

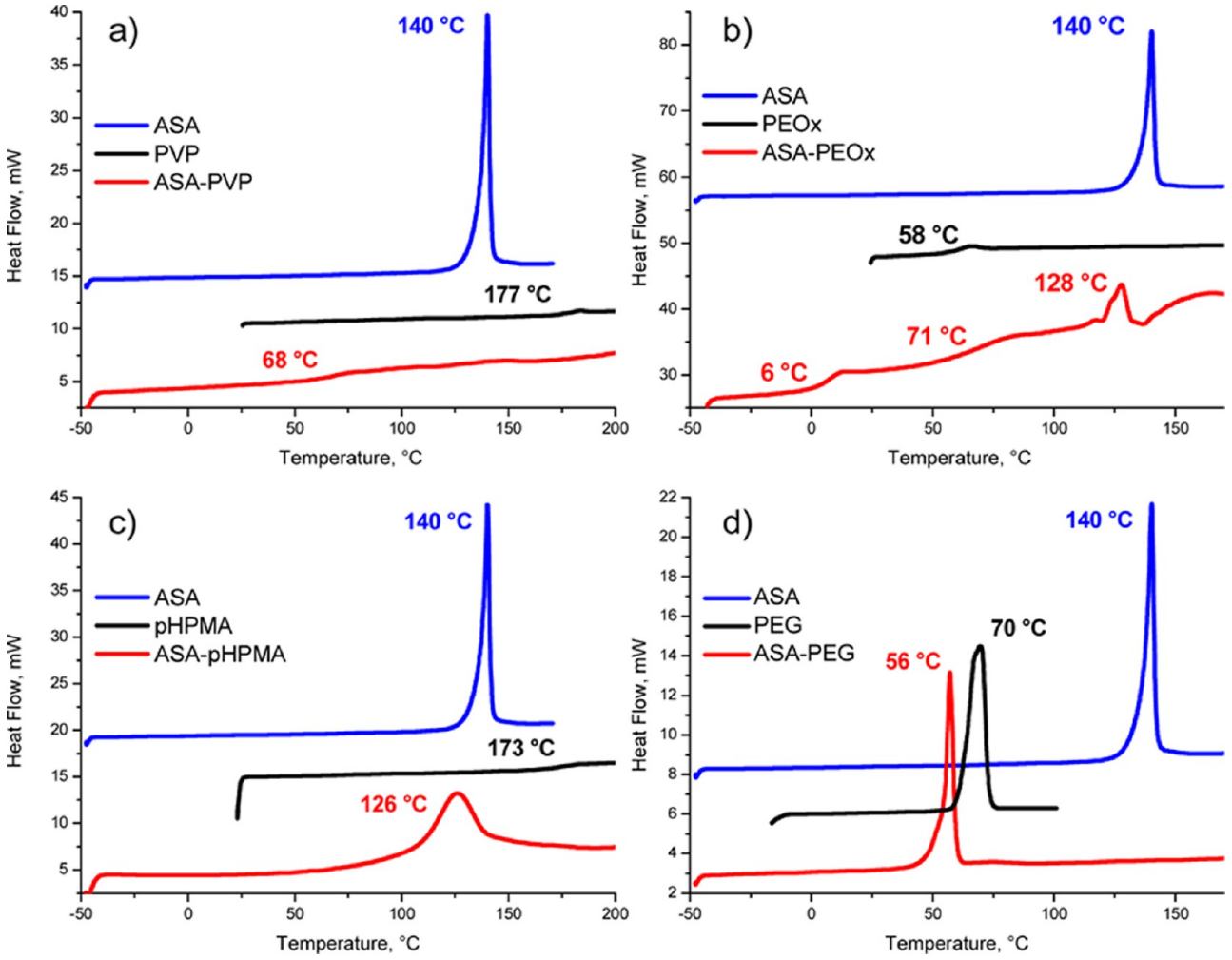

Figure 2. Comparison of DSC traces: the PVP–ASA solid dispersion, pure ASA, and pure PVP (a); PEOx–ASA solid dispersion, pure ASA, and pure PEOx (b); pHPMA–ASA solid dispersion, pure ASA, and pure pHPMA (c); and PEG–ASA solid dispersion, pure ASA, and pure PEG (d).

($PVP_{7600,40000,360000}$) were obtained from Fluka/Sigma-Aldrich (Buchs, Switzerland), while poly(2-ethyl-2-oxazolin) ($PEOx_{50000,200000,500000}$) was obtained from Sigma-Aldrich (St. Louis, USA). Synthesis of poly[*N*-(2-hydroxypropyl)-methacrylamide] (pHPMA) was done according to a procedure described in the literature.[20] Purity of all the prepared pHPMA polymers was more than 99.9% as determined by ^{1}H NMR spectroscopy. The M_w of pHPMA samples were 18 000, 54 000, and 81 000 with the corresponding polydispersities 1.16, 1.21, and 1.27, respectively. These values were determined by gel permeation chromatography in a mixture of acetate buffer (pH 6.5, 0.3 mol/L) and methanol (20:80 v/v) on a TSK 4000 column (Polymer Laboratories Ltd., U.K.) using a HPLC System Shimadzu (Shimadzu GmbH., Czech Republic) equipped with RI, UV, and multiangle light scattering DAWN DSP-F detectors (Wyatt, USA).

Preparation of Solid Dispersions. SDs of ASA were prepared by lyophilizing the prepared solutions at a wide range of percentage proportions of ASA/polymer from 10/90 to 80/20.[21,22] For further experiments, the ratio 30/70 was chosen due to most favorable properties of the dispersions (mechanical, physicochemical) while keeping drug loading as high as possible. First, 5% w/w solutions of ASA, $PVP_{7600,40000,360000}$, and $PEG_{2000,6000,10000}$ in *t*-but and 5% w/w solutions of $pHPMA_{18000,54000,81000}$ and $PEOx_{50000,200000,500000}$ in water were prepared. The prepared solutions were immediately mixed in a 30/70 weight ratio. The resulting mixtures were refrigerated for 5 h at −24 °C. The samples were freeze-dried on dishes (layer depth 5 mm) in a vacuum desiccator at 0.1 mbar overnight (16 h) at shelf temperature around −5 °C to create the solid dispersions. The polymers were dried before lyophilization, and each prepared solid dispersion was redried under high vacuum for 24 h. In all prepared SDs of ASA, there were no residual *t*-but and/or water detected by liquid state ^{1}H, ^{13}C NMR, and DSC.

Solid-State NMR (ss-NMR.). Solid-state NMR spectra were measured at 11.7 T using a Bruker Avance 500 US/WB NMR spectrometer (Karlsruhe, Germany, 2003). The following techniques were applied: (i) ^{1}H, ^{13}C, and ^{15}N MAS and CP/MAS NMR; (ii) measurements of ^{13}C-detected $T_1(^1H)$ and $T_{1\rho}(^1H)$ spin–lattice relaxation times;[23] (iii) ^{1}H–^{1}H ss-NMR correlation experiments such as ^{1}H–^{1}H DQ/SQ BABA,[24] ^{1}H–^{1}H SQ/SQ NOESY,[25] and ^{1}H–^{1}H SQ/SQ DUMBO,[26] (iv) ^{1}H–^{13}C wide-line separation (WISE),[27] (v) ^{1}H–^{13}C FSLG HETCOR,[28−30] and (vi) the measurements of ^{1}H–^{15}N dipolar profiles.[31] The frictional heating of the spinning samples was mitigated by active cooling, and temperature calibrations[32] were performed with $Pb(NO_3)_2$. Detailed experimental parameters are provided in Supporting Information S1.

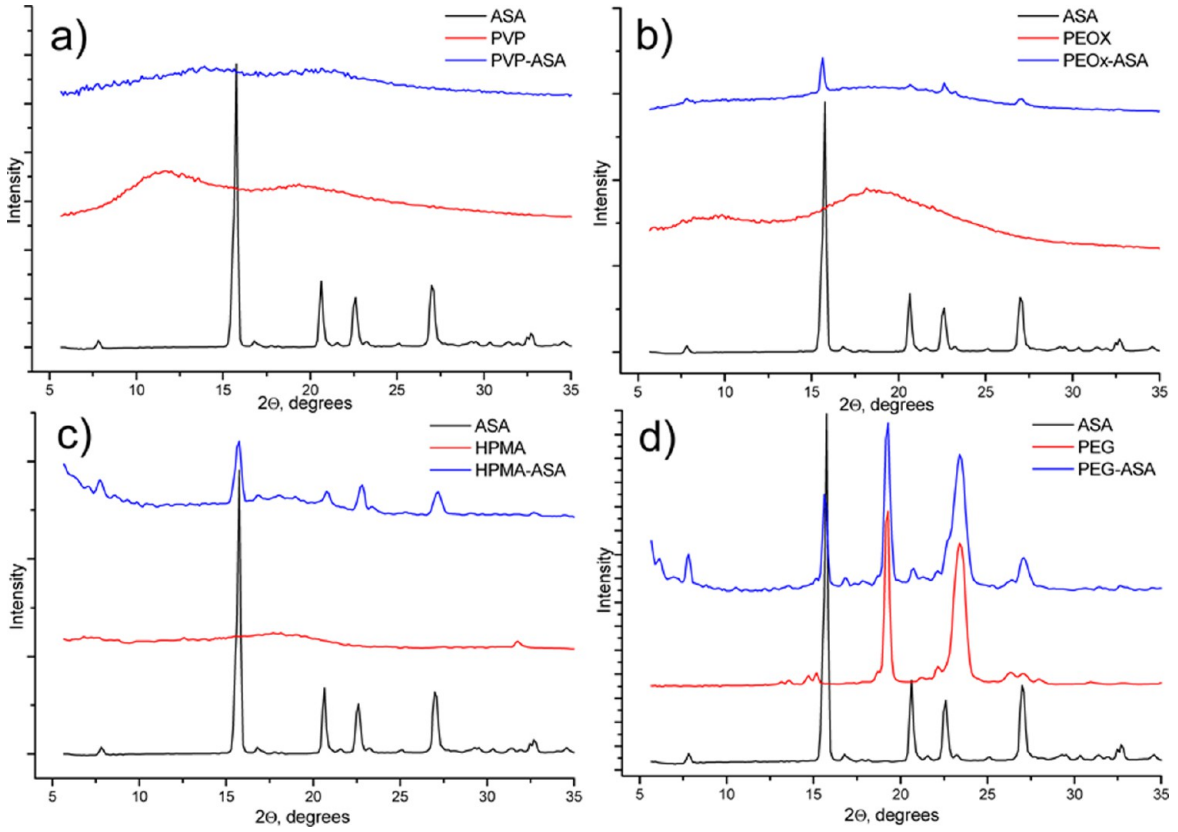

Figure 3. Comparison of WAXS patterns: PVP−ASA solid dispersion, pure ASA, and pure PVP (a); PEOx−ASA solid dispersion, pure ASA, and pure PEOx (b); pHPMA−ASA solid dispersion, pure ASA, and pure pHPMA (c); and PEG−ASA solid dispersion, pure ASA, and pure PEG (d).

Wide-Angle X-ray Scattering (WAXS). WAXS experiments were performed using a pinhole camera (Molecular Metrology System) attached to a microfocused X-ray beam generator (Osmic MicroMax 002) operating at 45 kV and 0.66 mA (30 W). The samples were measured in transmission mode using interchangeable 23 × 25 cm imaging plates (Fujifilm). The q range for the WAXS was 0.25−3.5 Å^{-1} ($q = (4\pi/\lambda) \sin \theta$, λ = 1.54 Å, and 2θ is the scattering angle). Calibration was conducted using Si powder. Quantitative analysis of WAXS patterns was performed using a software module "Analyze" (producer Seifert). Resulting crystallinity was calculated by the ration of integral intensity of the crystalline peaks and the integral intensity of all the peaks.

Differential Scanning Calorimetry (DSC). DSC analysis was performed on a Perkin-Elmer DSC 8500 calorimeter using nitrogen as the purge gas (20 cm^3/min). The instrument was calibrated for temperature and heat flow using indium. The samples (approximately 10 mg) were sealed inside hermetic aluminum crucibles with a single hole punched in the lid. An identical empty crucible was used as a reference. The DSC scans of each sample were performed at 20 °C/min from −50 to 200 °C. The glass transition temperatures were identified as the midpoint between the glassy and rubbery branches of the DSC trace, and the melting temperatures were the maxima of the corresponding endotherm plots.

RESULTS AND DISCUSSION

Differential Scanning Calorimetry. The primary phase-compositional information for the prepared solid dispersions was provided by the DSC measurements. Figure 2 displays the DSC thermograms for ASA, the polymer matrices, and the polymer−ASA systems. Pure ASA (form I[33]) exhibited a single, sharp melting endotherm at 140 °C (180 J/g), revealing its crystalline nature. All of the polymer matrices with the exception of PEG were amorphous, displaying a single T_g: PVP ≈ 177 °C, PEOx ≈ 58 °C, and pHPMA ≈ 173 °C. PEG displayed a crystalline structure with the melting at 70 °C.

Significant disparities in the DSC measurements were observed for the prepared SDs. Specifically, the T_g at ∼68 °C shifted toward lower temperatures[34] relative to pure PVP indicated the amorphous and basically homogeneous nature of the PVP-ASA systems. In contrast, the DSC trace with two T_gs and one endotherm revealed structurally much more complex multiphase composition of PEOx−ASA systems. The endothermic peak at 128 °C was attributed to ASA melting, whereas the two glass transitions revealed the two amorphous phases. The event at 70 °C most likely reflects the glass transition of the polymer-rich phase, while the T_g at 6 °C reflects the glass transition of a drug-rich PEOx−ASA phase. For pHPMA−ASA, no T_g was observed, most likely because it overlaps with the broad endothermic peak for ASA (T_m = 126 °C). In contrast, no endothermic peak that could be attributed to the melting of crystalline ASA was observed in the PEG−ASA solid dispersion, even though a high fraction of crystalline ASA was detected in this system by WAXS and ^{13}C CP/MAS NMR. As further confirmed by ultrafast DSC using the heating rates of 100, 200, and 300 °C/min, the absence of two endotherms in the DSC trace may be explained by the instant dissolution of ASA in the melted PEG during the DSC measurement.

Wide Angle X-ray Scattering. WAXS is one of the best tools for probing periodically ordered crystalline fractions in multicomponent polymeric solids.[35] Figure 3 compares the

WAXS diffractograms of pure ASA, the pure polymer matrices, and the prepared polymer−ASA solid dispersions. The pure ASA applied in this work was identified as the crystalline form I,[33] while the original PEOx and pHPMA were amorphous. PEG was a highly crystalline system with ca. 90% crystallinity.

As clearly demonstrated in Figure 3a, the prepared PVP−ASA solid dispersions are completely amorphous systems, while the low-intensity X-ray reflections detected for the PEOx−ASA systems (Figure 3b) indicate the presence of a residual crystalline ASA fraction. The quantitated crystallinity of this ASA fraction was approximately 5%, indicating that most of the ASA was dispersed in the PEOx matrix. In contrast, the diffractogram for the pHPMA−ASA formulation (Figure 3c) clearly revealed X-ray reflections indicative of polymorphic form I of ASA. The determined total crystallinity of the system reaching 30% indicated that ASA exclusively formed crystalline domains phase-separated from the amorphous pHPMA matrix. In the PEG−ASA systems the observed characteristic WAXS patterns (Figure 3d) together with the high total crystallinity (ca. 85%) revealed the existence of two distinct crystalline phases (PEG and ASA form I, respectively) and a residual amorphous phase.

Solid-State ^{13}C CP/MAS and ^{1}H MAS NMR Spectroscopy. The recorded ^{13}C CP/MAS NMR spectra (Figure 4) confirmed the results of the DSC and WAXS analyses and further elucidated the differences between the solid dispersions. In accordance with the WAXS experiments, the ASA molecules in the prepared PEG and pHPMA solid dispersions were characterized by narrow ^{13}C CP/MAS NMR signals, reflecting their crystalline nature. In contrast, for the PVP and PEOx solid dispersions, the corresponding ^{13}C CP/MAS NMR signals were broadened, indicating the disordered nature of ASA (Figure 4). In all cases, the structure of ASA was independent of the molecular weight of each applied polymer (Supporting Information S2−5).

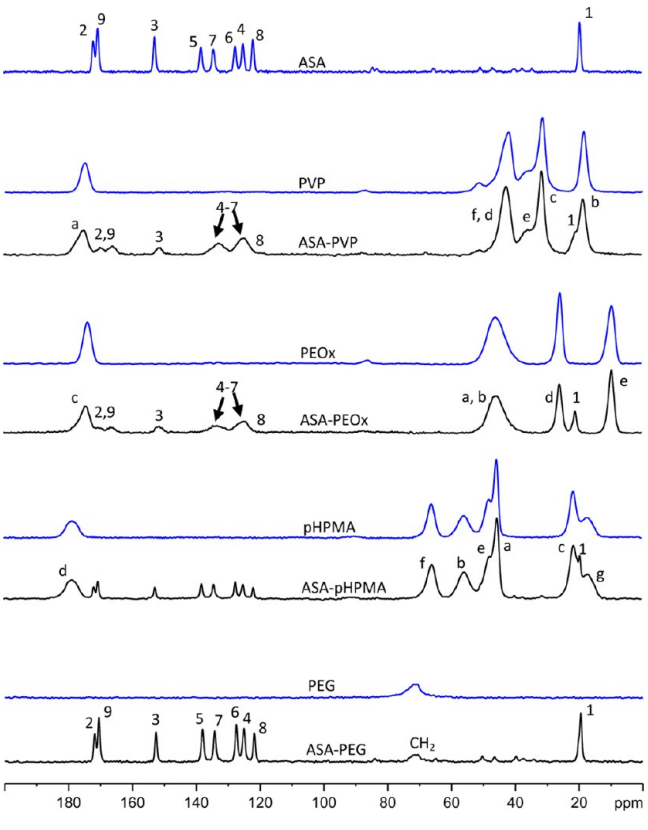

Figure 4. ^{13}C CP/MAS NMR spectra of ASA, the pure polymers (blue lines), and polymer−ASA solid dispersions in a 70/30 w/w ratio (black lines). The signal assignments for ASA were made based on the literature data[36] and ^{1}H−^{13}C FSLG HETCOR experiments.

A detailed inspection of the recorded spectra revealed molecular-level interactions between the ASA and certain polymer matrices. Initially, we detected the high-frequency shoulder in the ^{13}C CP/MAS NMR resonance frequency for the acetyl methyls of ASA at ca. 22 ppm in the PEG−ASA system (Figure 5a). The narrow signal at 70 ppm detected in the single-pulse ^{13}C MAS NMR spectrum (Supporting Information S6) indicated the presence of PEG liquid-like amorphous phase[37] (ca. 10−15% determined by spectral deconvolution). Nevertheless the dissolution of ASA in this phase was not confirmed because the corresponding narrow signals in ^{1}H MAS NMR spectra (Figure 6) were not detected. Therefore, the high-frequency shoulder on the ^{13}C CP/MAS NMR signals of the C1 methyl units in the PEG−ASA solid dispersions may be attributed to structural defects in the ASA crystallites induced by the crystalline PEG matrix (Figure 5).

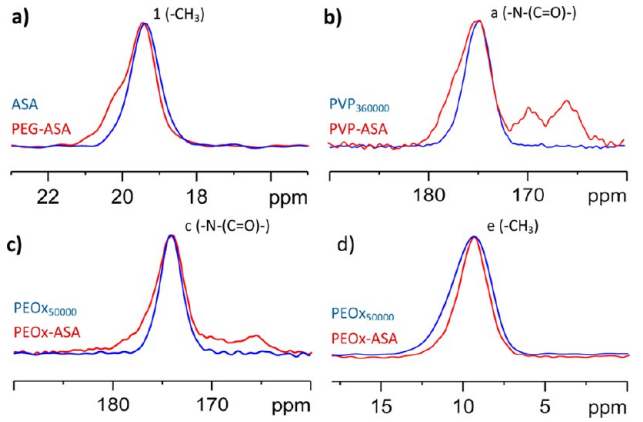

Figure 5. ^{13}C CP/MAS NMR spectra of solid dispersions expanded for PEG−ASA CH_3 units (a), PVP−ASA C═O units (b), PEOx−ASA C═O units (c), and PEOx−ASA CH_3 units (d).

The ^{13}C CP/MAS NMR signals for ASA in the PVP and PEOx dispersions exhibited extensive broadening and changes in the resonance frequencies approaching the ^{13}C NMR chemical shifts of ASA in acetone solution. Remarkably, the decrease in the chemical shift of the carboxyl carbon C9, $\Delta\delta$ = −4.6 ppm, revealed the decrease in hydrogen bonding strength involving the COOH groups. In contrast, the signals for the carbonyl carbons of PVP and PEOx were asymmetrically broadened by the shoulders in the high-frequency region with $\Delta\delta$ = +2−3 ppm (Figure 5b,c) indicating an increase in hydrogen bonding strength. Therefore, the hydrogen bonding interactions facilitating the incorporation of ASA into the PVP and PEOx polymer matrices[38] can be supposed. Unexpectedly, the ^{13}C CP/MAS NMR spectra of the PEOx−ASA dispersions displayed narrowing of CH_2 and CH_3 resonances in the PEOx chains (Figure 5d), indicating softening of the polymer matrix in the presence of ASA.

^{13}C-Detected T_1(^{1}H) and $T_{1\rho}$(^{1}H) Spin−Lattice Relaxation. In analogy with structural descriptions of polymeric composites and blends we focused on analyzing the ^{1}H−^{1}H spin-diffusion processes in order to obtain more insight into the

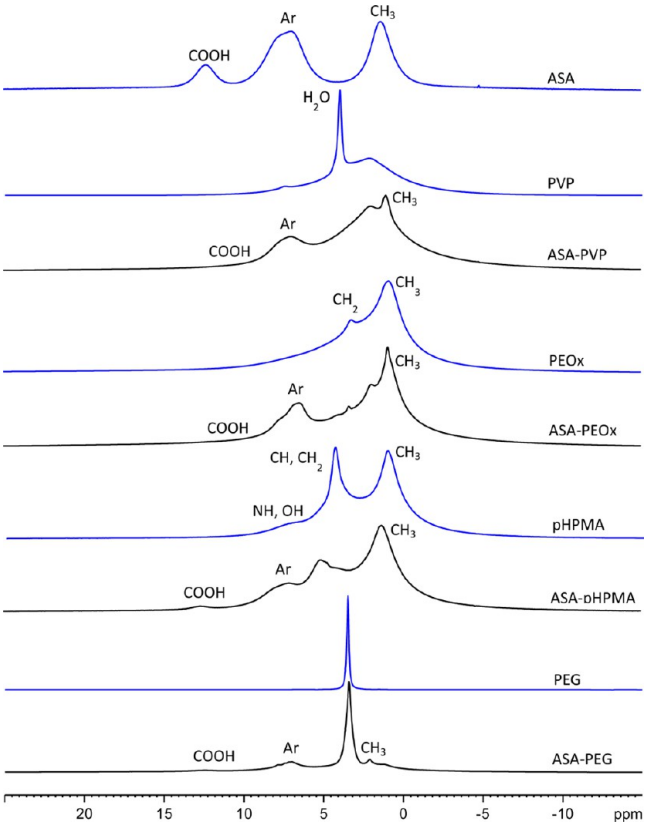

Figure 6. ^{1}H MAS NMR spectra of ASA, pure polymers (blue lines), and the corresponding polymer–ASA solid dispersions in a 70/30 w/w ratio (black lines).

distribution of ASA in polymeric matrices. There are numerous ss-NMR techniques,[39−42] which allow estimating the domain sizes from ca. 1 to 500 nm; however, the most robust one is based on the measurements of ^{1}H spin–lattice relaxation times in the laboratory and rotating frame, $T_1(^1\mathrm{H})$ and $T_{1\rho}(^1\mathrm{H})$, respectively. In this case, the ^{1}H–^{1}H spin diffusion, a fast magnetization transfer over large distances occurring during relaxation periods, induces ^{1}H magnetization behavior equilibration between different spins. The rate of this equilibration reflects the extent of phase separation. To approximately quantify the extent that the APIs were mixed with the polymer matrix, we estimated the maximum diffusive path length using the relaxation times. The maximum diffusive path length (L) obtained with the spin-diffusion in three dimensions over time (T_i) is as follows:[23,43−45]

$$L = (6DT_i)^{1/2} \quad (1)$$

where D is the spin-diffusion coefficient and T_i is either $T_1(^1\mathrm{H})$ or $T_{1\rho}(^1\mathrm{H})$. The typical value of the spin-diffusion coefficient for organic solids is 0.3–0.8 nm^2 ms^{-1}.[40] For the $T_{1\rho}(^1\mathrm{H})$ relaxation experiment, a 1/3 scaling factor should appear in the parentheses due to the reduced efficacy of spin diffusion during spin locking.[45] The relaxation data recorded for the systems representing each type of polymer matrix are summarized in Table 1. For the complete relaxation data for the systems with different M_w, see the Supporting Information S7–10.

As demonstrated in Table 1 both the $T_1(^1\mathrm{H})$ and $T_{1\rho}(^1\mathrm{H})$ of ASA were shorter in the PEG–ASA dispersions relative to pure crystalline ASA. The relaxation times also systematically decreased as the PEG M_w increased (Supporting Information S7). Although the $T_1(^1\mathrm{H})$ of ASA and PEG were not completely equilibrated, the observed decrease in $T_1(^1\mathrm{H})$ reflects the efficient transfer of ^{1}H magnetization between the ASA and PEG crystallites, indicating that ASA was incorporated into the polymer matrix. Another explanation of the observed reduction of $T_1(^1\mathrm{H})$ operates with the reduction of the particle size of ASA. Generally, the increase in the surface area of API particles can reduce $T_1(^1\mathrm{H})$ relaxation times due to the presence of higher amount of paramagnetic O_2 and due to the enhanced molecular mobility on the surface. To exclude this possibility we performed additional relaxation measurements using finely powdered pure crystalline ASA. The recorded $T_1(^1\mathrm{H})$ relaxation time (61 s), however, was almost identical with the original value (59 s). Therefore, we believe that the observed decrease in relaxation times going to ca. 20–30 s can be explained exclusively by the ^{1}H–^{1}H spin diffusion from the polymer matrix. Calculating L (eq 1) revealed that the ASA crystalline domains in PEG were ca. 300 nm.

Similarly, in pHPMA–ASA systems, the huge differences in the $T_{1\rho}(^1\mathrm{H})$ relaxation times of ASA and pHPMA (Table 1) revealed that the ^{1}H magnetization transfer did not reach a detectable rate within the applied ^{1}H variable pulses (tens of microseconds). Moreover, the $T_1(^1\mathrm{H})$ relaxation times for pHPMA in the solid dispersions remained unchanged relative to the pure polymers (ca. 1–2 s, Table 1 and Supporting Information S8). Although the slightly reduced $T_1(^1\mathrm{H})$ values determined for the ASA dispersed in pHPMA indicated partial equilibration of ^{1}H magnetization, the calculated maximum

Table 1. $T_1(^1\mathrm{H})$ and $T_{1\rho}(^1\mathrm{H})$ Relaxation Times Obtained for Pure ASA, PEG_{10000}, $pHPMA_{81000}$, PVP_{360000}, $PEOx_{500000}$, and the Corresponding SDs[a]

system		$T_1(^1\mathrm{H})$, s ASA	$T_1(^1\mathrm{H})$, s polymer	$T_{1\rho}(^1\mathrm{H})$, ms ASA	$T_{1\rho}(^1\mathrm{H})$, ms polymer
ASA	crystalline	59.0		370.0	
PEG_{10000}	semicrystalline		12.0		1.3
PEG_{10000}–ASA	crystalline/crystalline	20.0	3.8	323.0	0.4
$pHPMA_{81000}$	amorphous		1.0		5.1
$pHPMA_{81000}$–ASA	amorphous/crystalline	31.0	1.0	363.0	4.3
PVP_{360000}	amorphous		2.9		25.1
PVP_{360000}–ASA	amorphous/amorphous	4.2	4.3	10.2	9.8
$PEOx_{500000}$	amorphous		3.5		10.9
$PEOx_{500000}$–ASA	amorphous/amorphous	2.5	2.5	4.1	4.0

[a]The ^{13}C-detected $T_1(^1\mathrm{H})$ and $T_{1\rho}(^1\mathrm{H})$ relaxation times were calculated for each resolved signal. The reported values were extracted from the signals of the C4, C6, and C8 aromatic carbons in ASA, the CH_2 unit of PEG, the CH_2 unit (a,e) of pHPMA, the CH_2 unit (e) of PVP, and the CH_2 unit (a,b) of PEOx. The relaxation curves were fitted with a single-component exponential decay.

dx.doi.org/10.1021/mp400495h | Mol. Pharmaceutics 2014, 11, 516–530

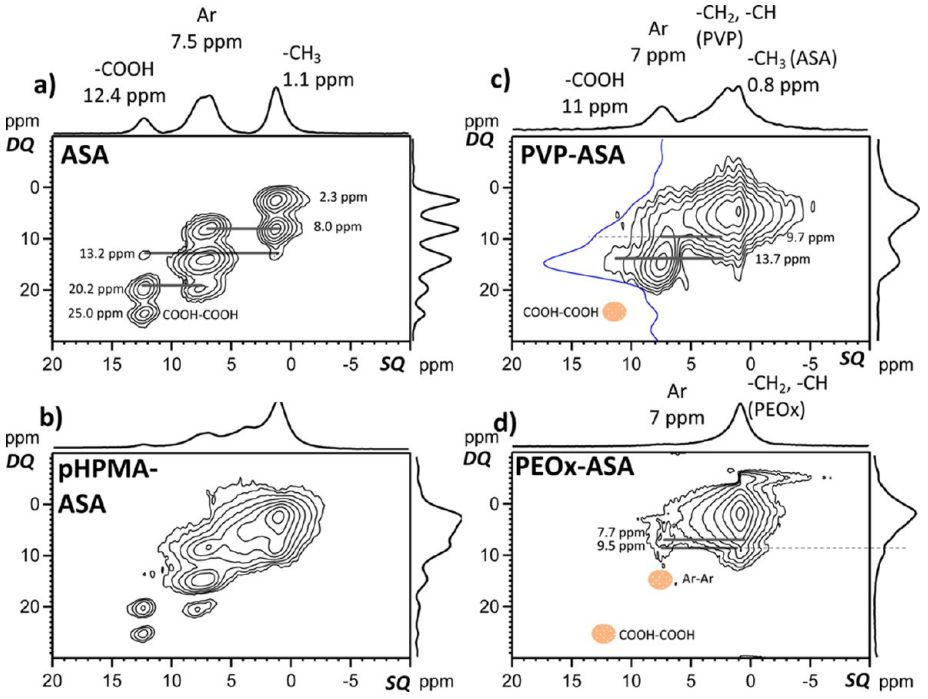

Figure 7. $^{1}H-^{1}H$ DQ/SQ MAS NMR spectra (30 kHz) of ASA in crystalline form I (a); in a 30% w/w amorphous dispersion with pHPMA (b); in a 30% w/w amorphous dispersion with PVP (c); and in a 30% w/w amorphous dispersion with PEOx (d). The correlation signals and ^{1}H chemical shifts are indicated.

diffusive path length (L) indicated large dimensions of ASA crystallites in the pHPMA matrix (>400 nm).

In contrast, for the PVP−ASA and PEOx−ASA systems, the recorded $T_1(^{1}H)$ and $T_{1\rho}(^{1}H)$ relaxation times for ASA were basically identical to the relaxation times recorded for the PVP and PEOx matrices (Table 1, Supporting Information S9 and S10). Because no significant differences were observed between systems with different M_w, both types of solid dispersions could be considered as basically homogeneous on the nanometer scale.

2D $^{1}H-^{1}H$ Homonuclear Correlation Spectroscopy. To probe detailed subnanometer structural motifs in solid dispersions, the experiments combining site-specific information with the fine control of ^{1}H polarization transfer had to be applied. In this respect, the $^{1}H-^{1}H$ correlation techniques employing $^{1}H-^{1}H$ spin diffusion or the evolution of ^{1}H double-quantum (DQ) coherences are preferred due to their relatively high sensitivity. One of the most robust techniques is $^{1}H-^{1}H$ DQ/SQ MAS NMR,[24] in which a DQ correlation signal typically indicates a proton−proton distance under 3.5 Å. Therefore, the straightforward interpretation of $^{1}H-^{1}H$ DQ/SQ MAS NMR spectra that may provide direct evidence of the intimate intermolecular contacts is usually the first choice for elucidating the miscibility of pharmaceutical SDs at the molecular level.[46]

A well-resolved $^{1}H-^{1}H$ DQ/SQ MAS NMR spectrum with all of the expected correlation signals was recorded for crystalline ASA, form-I (Figure 7a). By using the corresponding X-ray diffraction data (Crystallographic Information File, CSD refcode: ACSALA02)[33] we were able to calibrate $^{1}H-^{1}H$ interatomic distances that can be probed by this type of experiment. Specifically, the autocorrelation signal for the COOH protons at δ_{DQ} = 25 ppm (in DQ dimension), which reflects the dimeric arrangement of the hydrogen-bonded ASA molecules, was perfectly evolved. The corresponding distance between the neighboring COOH protons in the crystal lattice derived from diffraction data[33] is 2.46 Å. The recorded spectrum also allowed us to estimate the maximum $^{1}H-^{1}H$ distance that could be detected under these experimental conditions. The weak correlation signals at δ_{DQ} = 13.2 ppm between the COOH and CH_3 groups indicate that this distance is approximately 3.6 Å.

Comparing the results obtained for pure ASA with the spectra recorded for the prepared dispersions revealed three remarkable differences (Figure 7b−d). First, the spectral resolution decreased significantly as a result of amorphous character of polymer matrices. Second, the autocorrelation signals for COOH protons disappeared in the PVP−ASA and PEOx−ASA systems, indicating that molecules of ASA no longer adopt hydrogen-bonded dimeric motifs C═O(OH)···O═C(OH) (Figure 7c,d). The carboxyl groups of ASA molecules in PVP−ASA systems are separated by more than 3.6 Å. Third, the absence of autocorrelation DQ signals for the aromatic protons of ASA in the PEOx−ASA dispersions indicated the release of high-amplitude motions (Figure 7d).

To overcome the problem with the reduced efficacy of DQ coherence excitation, the NOESY-type $^{1}H-^{1}H$ SQ/SQ MAS NMR techniques were applied. The capability of these experiments arises from the fact that excitation of single-quantum (SQ) coherences is relatively easy and the polarization transfer between the neighboring spins is driven by strong $^{1}H-^{1}H$ dipolar couplings. Consequently, the polarization transfer is efficient even in semiflexible polymeric systems.[25]

As demonstrated on the aromatic and carboxyl protons of crystalline ASA, the detectable correlation signals revealing protons in close proximity evolved within 0.5−1.0 ms of the polarization transfer (see Supporting Information S11). Complete evolution of the correlation signals, however, remained incomplete even after 50 ms. Moreover, the

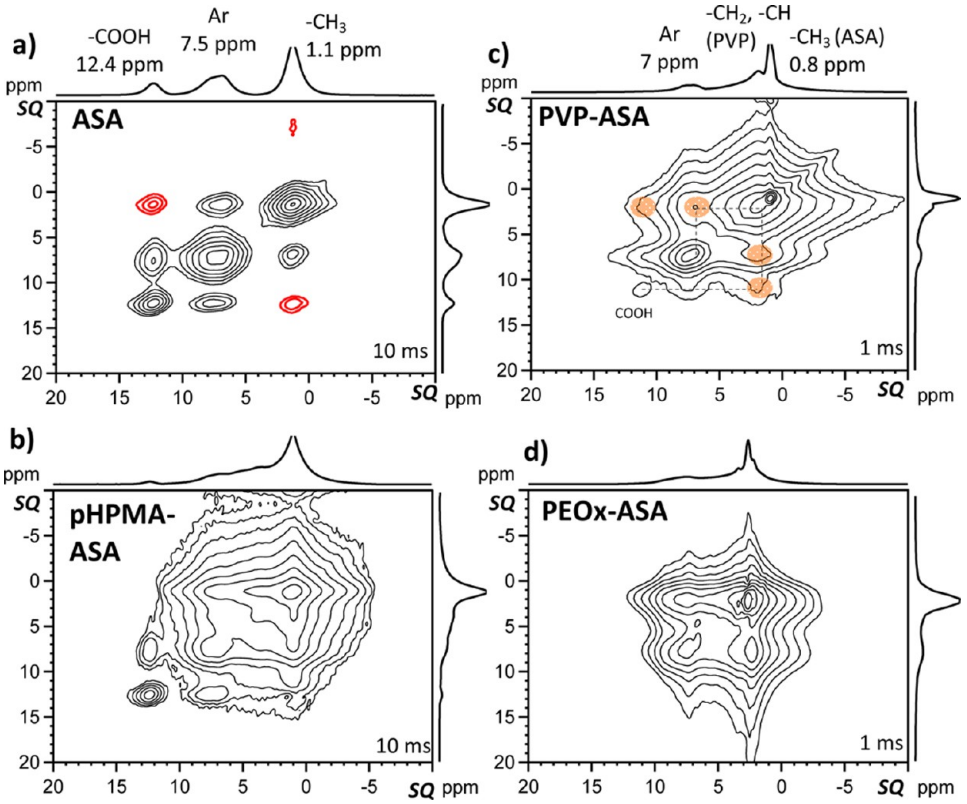

Figure 8. $^{1}H-^{1}H$ SQ/SQ MAS NMR spectra (30 kHz) of ASA in crystalline form I (a); in a 30% w/w amorphous dispersion with pHPMA (b); in a 30% w/w amorphous dispersion with PVP (c); and in a 30% w/w amorphous dispersion with PEOx (d). The spectra were measured with spin-diffusion mixing times of 10 and 1 ms, as indicated.

correlations between the methyl and carboxyl protons, corresponding to a separation of 3.6−4.8 Å, were negative (Figure 8a). This behavior probably arising from the relayed NOE-driven polarization transfer[47] between the weakly coupled protons involving rapidly rotating methyl groups of ASA[48] under fast MAS (30 kHz) unpredictably modulates the build-up of correlation signals.[49] This complex magnetization behavior thus precludes reliable interpretation of the $^{1}H-^{1}H$ SQ/SQ MAS NMR spectrum for the pHPMA−ASA system because the correlation pattern typical for crystalline ASA is overlapped with that of amorphous pHPMA (Figure 8b). In this way, subtraction and cancellation of correlation signals can be expected.

In contrast, for the PVP−ASA solid dispersions the correlation signals between the aromatic protons of ASA and the CH_2/CH segments of PVP clearly evolved within 1 ms (Figure 8c). Similarly, the correlations between the carboxyl protons of ASA and the protons of PVP were easily detected, indicating the active role of carboxyl groups in tight incorporation of ASA into the PVP matrix. After applying the same experimental conditions for PEOx−ASA, we detected broad correlation signals involving aromatic protons from ASA; however, no correlations involving carboxyl units were detected. Moreover, the signals indicating polarization transfer between ASA and PEOx were very weak (Figure 8d). This finding thus indicate that segmental motions in PEOx−ASA combined with relatively fast MAS (30 kHz) significantly suppress static dipolar couplings to effective in polarization transfer processes. Therefore, structural elucidation of PEOx−ASA semiflexible polymeric systems must be performed at much slower spinning speeds (ca. 7−12 kHz).

This requirement can be achieved by the application of the experiments with ^{1}H homodecoupling sequences such as FSLG[28] or DUMBO[26] providing sufficient spectral resolution. In this respect, the 2D $^{1}H-^{1}H$ SQ/SQ DUMBO experiment rotor-optimized for moderate spinning frequencies (10−12kHz) is an optimal choice because it provides ultimate ^{1}H spectral resolution, keeps $^{1}H-^{1}H$ polarization transfer fast and efficient, and allows time-saving data acquisition due to the direct detection of ^{1}H magnetization.

These assumptions are demonstrated in the $^{1}H-^{1}H$ SQ/SQ DUMBO MAS NMR spectrum of ASA (Figure 9a); the correlations reflecting medium-range intermolecular contacts involving aromatic, carboxyl, and methyl protons are well evolved after a relatively short mixing period (500 μs). The same mixing time also yielded positive correlation signals for the long-range intermolecular contacts between the methyl and carboxyl protons. Consequently, the presence of strong correlation signals in the spectra measured with a 500 μs mixing period is indicative for intimate intermolecular contacts. In contrast, the absence of correlations between different molecules confirms some types of phase separation. This situation is well demonstrated in the spectrum of the pHPMA−ASA dispersion that was measured using a mixing period of 1−3 ms length (Figure 9b). Because of the significantly enhanced spectral resolution, two separate correlation patterns were identified: one for ASA and one for pHPMA. However, no correlation signal indicating the intercomponent contact was observed. In contrast, such correlation signals between CH_3 groups of ASA and CH_2 protons of PEG chains (Figure 9c) evolved after 3 ms of the spin-diffusion mixing indicating thus specific ASA−PEG interactions on the interfacial area.

dx.doi.org/10.1021/mp400495h | *Mol. Pharmaceutics* 2014, 11, 516−530

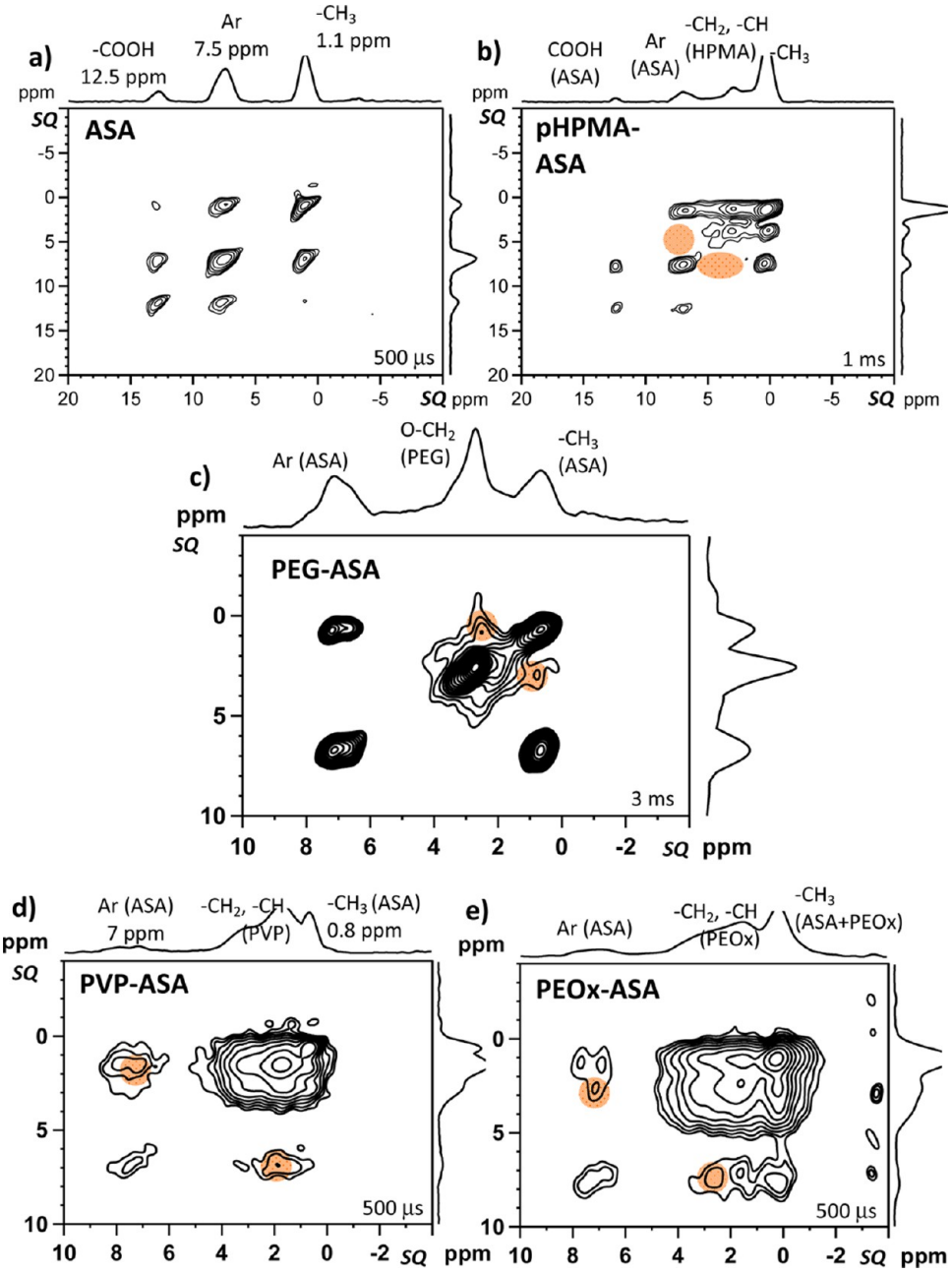

Figure 9. $^{1}H-^{1}H$ SQ/SQ DUMBO NMR spectra (10 kHz) of ASA in crystalline form I (a); in a 30% w/w amorphous dispersion with pHPMA (b); in a 30% w/w amorphous dispersion with PEG (c); in a 30% w/w amorphous dispersion with PVP (d); and in a 30% w/w amorphous dispersion with PEOx (e). The spectra were measured with spin-diffusion mixing times of 3 and 1 ms and 500 μs as indicated.

The use of DUMBO homodecoupling sequences significantly enhanced the spectral resolution even for the completely amorphous PVP−ASA and PEOx−ASA systems, allowing us to resolve the CH_3 resonances of ASA from the aliphatic protons of the polymers (Figure 9d,e). This resolution enhancement particularly apparent for PEOx−ASA (Figure 9e) resulted in clear detection of strong correlations between ASA and the polymer matrices, confirming thus molecular-level mixing in both PVP−ASA and PEOx−ASA dispersions.

^{15}N CP/MAS NMR Spectroscopy and Measurements of $^{1}H-^{15}N$ Dipolar Profiles. The hydrogen-bonding activity of carboxyl groups is often probed using FTIR and ^{13}C CP/MAS NMR spectroscopy.[38] However, the role of N−CO moieties of the polymers may be more complex and therefore should be probed complementarily for instance by assessing changes in the ^{15}N CP/MAS NMR chemical shifts.[50] For the PVP−ASA and PEOx−ASA dispersions, the ^{15}N CP/MAS NMR spectra exhibited high-frequency shoulders for the −N−(C═O)− signals at 137.2 and 121.6 ppm, respectively (Figure 10). Furthermore, in spite of the low signal-to-noise ratio, the $^{1}H-^{15}N$ dipolar profiles[31] measured for PVP−ASA and PEOx−ASA exhibited a slightly faster depolarization rate than those observed for the parent polymers (Supporting Information S12) indicating increased proton density in the vicinity of nitrogen sites. To unambiguously confirm the existence of weak H-bond interactions between ASA and the −N−(C═O)− segments of PVP and PEOx FTIR spectra were recorded (see Supporting Information S13). In accord with the comple-

dx.doi.org/10.1021/mp400495h | *Mol. Pharmaceutics* 2014, 11, 516−530

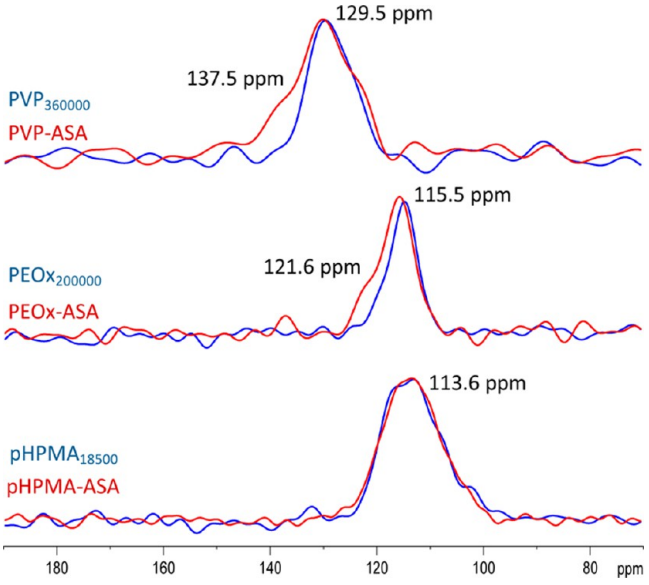

Figure 10. ^{15}N CP/MAS NMR spectra of parent polymers (blue lines) and the polymer−ASA dispersions (red lines).

mentary quantitative analysis of the corresponding ^{13}C CP/MAS NMR spectra (signals of carbonyl groups) the deconvolution of the ^{15}N CP/MAS NMR signals (Figure 10) confirmed that ca. 25 and 20% of the monomer units were involved in hydrogen bonding in PVP−ASA and PEOx−ASA dispersions, respectively. Considering the molar ratio of monomer units and ASA (PVP/ASA = 3.8/1 and PEOx/ASA = 4.3/1), this finding indicates that majority of ASA molecules is hydrogen bonded with the polymer matrix. In contrast, no H-bonding was detected in pHPMA−ASA systems.

2D ^{1}H−^{13}C Heteronuclear Correlation Spectroscopy. The 2D ^{1}H−^{13}C wide-line separation (WISE) NMR experiment[27] is a suitable technique for correlating the structure, mobility, and morphological information in heterogeneous polymer materials. Differences in molecular mobility are probed by ^{1}H line shapes, which are separated in the second dimension by the ^{13}C chemical shift: highly flexible segments generate narrow ^{1}H lines, while rigid units produce broad ^{1}H signals.

The analysis of the ^{1}H−^{13}C WISE NMR spectra (Figure 11a,b) revealed three remarkable differences between PVP−ASA and PEOx−ASA systems. First, the ^{1}H wide-line spectrum of aromatic ═CH− units of ASA was significantly broader for PVP−ASA than that for PEOx−ASA systems (Figure 11c). This finding definitely confirmed high-amplitude motions of ASA in PEOx−ASA dispersions. Second, the ^{1}H wide-line spectra of aromatic units of ASA and methylene segments of PVP recorded for PVP−ASA dispersions were identical (Figure 11d) reflecting thus the highly homogeneous nature of the system. The molecules of ASA adopt motional behavior of PVP chains and vice versa. In contrast, the ^{1}H wide-line spectra extracted for different PEOx−ASA segments exhibited variable broadening. While the ^{1}H spectrum of ═CH− units of ASA was narrow, considerable broadening was observed for the ^{1}H wide-line spectra of CH_2 units of PEOx (Figure 11e). Moreover, these spectra exhibited a two-component character with superimposed narrow and broad lines indicating motional heterogeneities in PEOx matrix. This fact suggested that ASA molecules and a fraction of PEOx segments were relatively mobile, while the rest of the PEOx chains remained rigid.

As the molecules of ASA do not entirely adopt the motional behavior of PEOx, local clustering must be expected. To probe this phenomenon in detail, we utilized ^{1}H−^{13}C FSLG HETCOR NMR spectroscopy that combines high spectral resolution with an efficient ^{1}H polarization transfer. As recently demonstrated, even the simple Hartman−Hahn (HH) cross-polarization (CP) step enables relatively fine control over the distance at which ^{1}H magnetization is transferred. Typically, most correlations observed at HH−CP contact times <110−150 μs correspond to ^{1}H−^{13}C distances <2.5 Å, while the

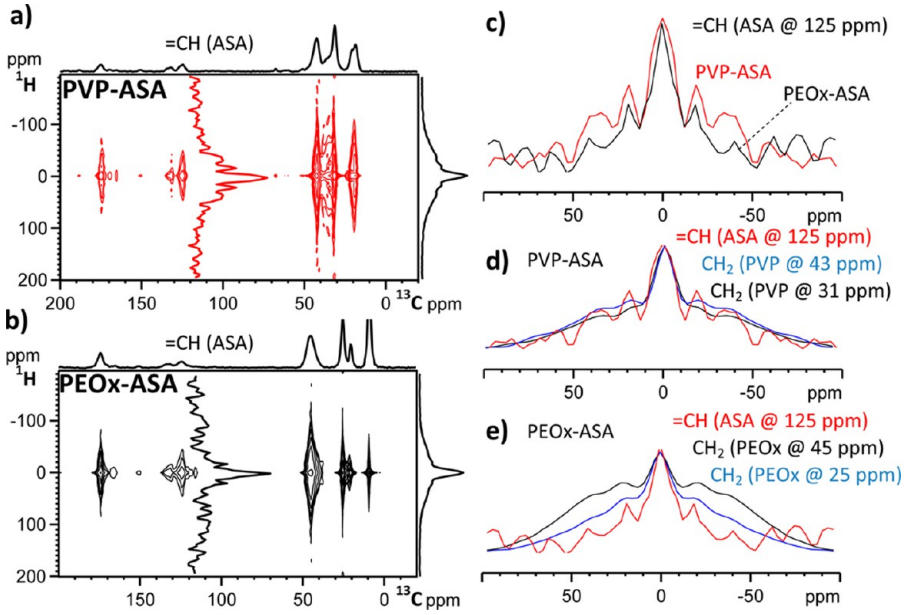

Figure 11. ^{1}H−^{13}C WISE NMR spectra of ASA in a 30% w/w amorphous dispersion with PVP (a) and in a 30% w/w amorphous dispersion with PEOx (b); an overlay of the ^{1}H wide-line spectra separated for the aromatic ═CH units from ASA in PVP−ASA and PEOx−ASA (c); overlay of the ^{1}H wide-line spectra separated for the aromatic ═CH units from ASA and the CH_2 groups from PVP in PVP−ASA (d); and overlay of the separated ^{1}H wide-line spectra for the aromatic ═CH units from ASA and the CH_2 groups from PEOx in PEOx−ASA (e).

dx.doi.org/10.1021/mp400495h | *Mol. Pharmaceutics* 2014, 11, 516−530

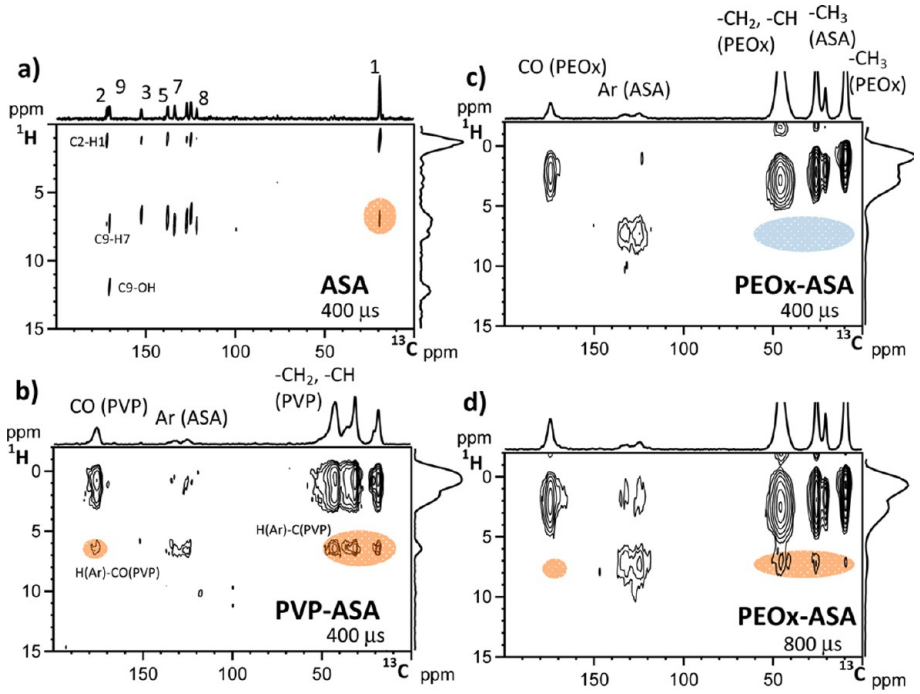

Figure 12. ^{1}H−^{13}C FSLG HETCOR NMR spectra of ASA in crystalline form I (a); in a 30% w/w amorphous dispersion with PVP (b); and in a 30% w/w amorphous dispersion with PEOx (c,d). The spectra (a−c) were recorded with 500 μs of CP, while spectrum (d) was recorded with 800 μs of CP.

medium-range ^{1}H−^{13}C contacts of ca. 3.0 Å requires usually 300 μs.[51] As in the case of crystalline ASA, these times, however, are a bit longer if the polarization transfer involves flexible segments. For instance the correlation signals between the rapidly rotating methyls and aromatic protons (δ_{1H} = 7 and δ_{13C} = 17 ppm) separated by about 3.0 Å required a 400 μs contact time (Figure 12a).

After applying the same 400 μs HH−CP period, the correlation signals reflecting polarization transfer from ASA to the polymer matrix were detected only for PVP−ASA (Figure 12b), while for the PEOx−ASA systems, the detection of the corresponding signals required the 800 μs mixing time (Figure 12c). Complete evolution of these correlations was attained after 2 ms (Figure 12d). These facts thus definitely confirm that ASA molecules are not entirely dispersed in the PEOx matrix on molecular level but instead locally form certain clusters. However, shown by applying the spin-diffusion coefficient reflecting the enhanced segmental dynamics of ASA (D = 0.4 nm^2 ms^{-1}), the size of these clusters calculated according the eq 1 is relatively small, not larger than ca. 1.2−1.3 nm.

Methodological Approaches in Structure Evaluation of Solid Dispersions. Generally, API molecules may exist in solid dispersions as separated amorphous or crystalline phases; they may also be present in an intimate mixture with the polymer in which the degree of contact may vary from fully miscible glass solutions to partly separated nanodomains. Because of the complexity of solid dispersions, precise structural characterization is very complicated; and in some cases, individual experimental methods may provide seemingly inconsistent results.

The most prominent example of such inconsistent data can be demonstrated on PEOx−ASA systems for which the DSC and WAXS measurements found a minor fraction of crystalline ASA, while ^{13}C CP/MAS NMR detected ASA only in the amorphous phase. This contradiction most likely occurs due to the combination of two factors. First, the amount of crystalline ASA in the PEOx−ASA system is relatively low (ca. 5%); second, the T_1(^{1}H) relaxation time is long (ca. 60 s). Complete magnetization recovery therefore requires 300 s between consecutive scans, making high-quality ^{13}C CP/MAS NMR spectra impractical to obtain. Consequently, the experimental ^{13}C CP/MAS NMR spectra measured with short repetition delays are dominated by the signals of rapidly relaxing amorphous ASA fractions, while the signals of the crystalline ASA are suppressed. The second example is represented by PEG−ASA systems for which even the ultrafast DSC data showed a single endothermic event indicating homogeneous cocrystalline-like character, whereas the WAXS and ss-NMR data revealed existence of separated crystalline domains of ASA embedded in crystalline PEG matrix.

Describing solid dispersions thus requires combinations of many experimental approaches. Relatively fast and reliable procedure allowing primary structural characterization involves combination of DSC, WAXS, ^{13}C CP/MAS NMR spectroscop,y and the measurements of ^{13}C-detected T_1(^{1}H) spin relaxation times. In this way distinct types of solid dispersions can be distinguished and homogeneity of the systems in the scale of ca. 10−500 nm can be probed. Although the spatial information derived from relaxation experiments is relatively rough, the robustness of these experiments make them the first choice in characterizing homogeneity of solid dispersions.

To obtain detailed structural information in nanometer and subnanometer scale the techniques of homonuclear and heteronuclear correlation ss-NMR spectroscopy must be used. Moreover, because of the hardly predictable motional state of solid dispersions a combination of correlation experiments employing different ways of polarization transfer under different regimes (e.g., ^{1}H spin-diffusion, ^{1}H DQ excitations, ^{1}H−^{13}C HH−CP, etc.) is an optimal choice because each of them provides a bit different structural information. In this respect it

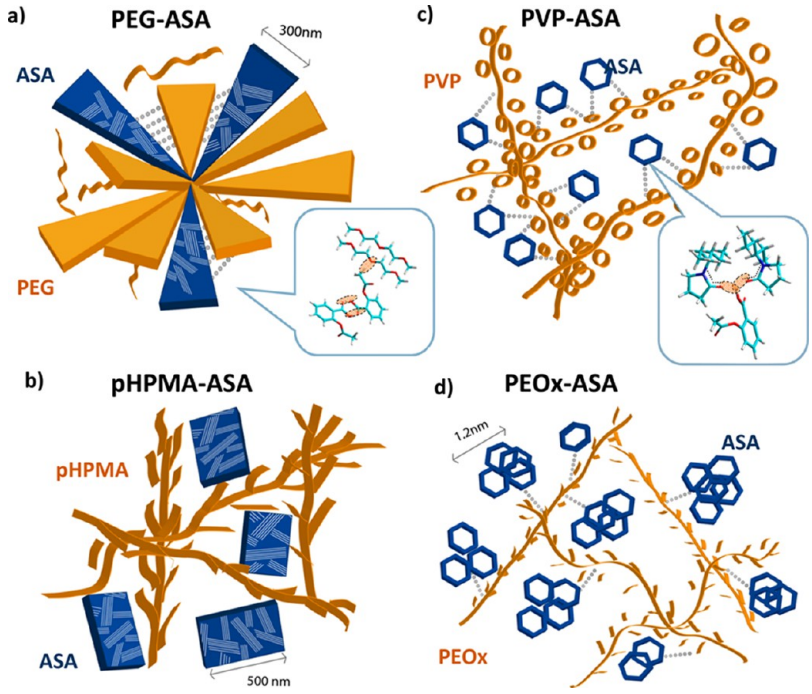

Figure 13. Schematic representation of distinct types of polymer−ASA solid dispersions: (a) PEG−ASA crystalline solid dispersions; (b) pHPMA−ASA amorphous solid dispersions (glass suspensions); (c) PVP−ASA solid solutions; and (d) PEOx−ASA nanoheterogeneous solid solutions/suspensions.

is worthy to note that the existence of nanometer-sized motional heterogeneities in PEOx−ASA was clearly revealed by one of the most robust and easy to implement techniques such as the $^{1}H-^{13}C$ WISE experiment.

Considering the existence of hydrogen bonds in the systems the analysis of ^{1}H, ^{13}C, and ^{15}N NMR signals of the key N−CO and COOH moieties can provide primary evidence. However, the relatively small changes observed in the chemical shifts may have many causes other than hydrogen bonding. Therefore, additional proofs are required. The recently developed 2D $^{14}N-^{1}H$ HSQC and $^{1}H-^{17}O$ CP-HETCOR NMR experiments would be a perfect choice; however, the hardware requirements, including very high magnetic fields, sample spinning faster than 50 kHz,[52] and/or isotopic labeling,[42] preclude the execution of these experiments with standard equipment. In this respect we tested measurements of $^{1}H-^{15}N$ dipolar profiles under CPPI conditions. Although this experiment is relatively time-consuming, the changes in the proton distributions near the nitrogen sites can be easily evaluated in terms of hydrogen bonding.

Structural Diversity of the Solid Dispersions of ASA. Using the above-discussed experiments, four distinct types of solid dispersions of ASA were resolved and desribed: (i) crystalline solid dispersions containing ASA nanocrystallites (ca. 300 nm) in a crystalline PEG matrix (Figure 13a); (ii) amorphous solid dispersions (glass suspensions) with ASA crystallites (>450 nm) embedded in an amorphous pHPMA matrix (Figure 13b); (iii) solid solutions with molecularly dispersed ASA in a rigid amorphous PVP matrix (Figure 13c); and (iv) nanoheterogeneous solid solutions/suspensions containing nanosized ASA clusters (ca. 1−2 nm) dispersed in a semiflexible PEOx matrix (Figure 13d). In all cases, the type and structure of solid dispersions of ASA were controlled by the chemical constitution of the applied polymers, while varying the M_w had no effect. In this respect, it is noteworthy that all four systems were prepared using the same freeze-drying procedure. Freeze-drying, although less commonly used in the industry due to its relative expensiveness, allows the preparation of solid dispersions in a very wide range of parameters. Application of other techniques such as spray drying or melt quenching could potentially lead to the formation of completely different 3D architecture.

Structural diversity of solid dispersions generally arises from weak, reversible van der Waals interactions, which control the drug and polymer segments' assembly. Two types of active sites can be found in PEG. Oxygen $-CH_2-\underline{O}-$ atoms are hydrogen bonding acceptors while the slightly positively charged $-C\underline{H}_2-O-$ protons facilitate hydrophobic interactions.[53] In contrast, the nitrogen atoms and carbonyl groups in −N−(C═O)− moieties of PVP and PEOx act as hydrogen bonds acceptors, while the −NH−(C═O)− amide group of pHPMA is both donor (NH) and acceptor (CO) of protons.

As followed from our experiments, the interactions between the hydrogen-bond acceptors of PEG and pHPMA and −COOH protons of ASA are too weak to keep the molecules of ASA molecularly dispersed in polymer matrix. Regardless of the different physicochemical properties of PEG and pHPMA, the self-aggregation occurs, leading to the crystallization of ASA in the phase-separated domains. However, there are certain experimental evidence, such as single melting temperature and broadening of ^{13}C CP/MAS NMR methyl signal of ASA, that indicate slight interdomain interactions between the crystallites of ASA and spherulites of PEG. In analogy of catemeric structural motifs found in the crystalline lattice of ASA (forms I and II)[54] and bearing in mind the observed slight correlations in the $^{1}H-^{1}H$ DUMBO NMR spectrum (Figure 9c) these interdomain interactions can be provided by the surface methyls of acetyl groups of ASA and $-CH_2-O-$ units of PEG. Because of these interactions the molecules of ASA can

dx.doi.org/10.1021/mp400495h | Mol. Pharmaceutics 2014, 11, 516−530

preferentially crystallize in the interlamellar spaces of PEG spherulites (Figure 13a).

In contrast to PEG and pHPMA, the nonprotonated −N−(C═O)− moieties in PVP and PEOx enabled efficient interactions with the −COOH protons. Analogous to the structure of borneol−PVP nanocomposites,[55] the ASA molecules can be coordinated by the two carbonyl groups of PVP (Figure 13c). Because of the delocalization of the nitrogen lone pair within the −N−(C═O)− moiety, larger hydrogen bonding clusters, possibly involving water molecules, may be created. Consequently, homogeneous solid solutions of ASA occurred in the PVP matrix. Probably, because of the slightly higher segmental mobility of PEOx and/or steric effects, the hydrogen bonding between −N−(C═O)− sites of PEOx and the protons of ASA are weakened. Because of low T_g of ASA (T_g = −30 °C), the amorphization of ASA requires at room temperature stabilization via hydrogen-bonding and steric interactions with excipients. Without this stabilization, ASA molecules exhibit high amplitude rotational diffusion motions, act as a plasticizer, and can migrate through the polymer matrix. These facts may result in concentration fluctuations of the mobile molecules ASA in amorphous PEOx matrix. Consequently, the resulting PEOx−ASA systems are nanoheterogeneous, with a flexible drug-rich phase (T_g = 6 °C) and a rigid polymer-rich phase (T_g = 70 °C). As the sufficiently large clusters of ASA can start to recrystallize, multiple states of ASA in PEOx−ASA systems were detected.

CONCLUSIONS

In this contribution we demonstrated that the 3D architecture of solid dispersions of ASA prepared by freeze-drying is primarily controlled by the chemical nature of polymer matrices, while the molecular weights of these polymers have limited structural impact. Four distinct types of ASA solid dispersions including crystalline solid dispersions, amorphous glass suspensions, and two types of solid solutions were identified and structurally described in detail. Our experimental findings confirm that structural properties of these systems are determined by a combination of two factors: (i) the accessibility and affinity of suitable molecular sites for forming hydrogen-bond interactions between the API and the polymer matrix; and (ii) the segmental dynamics and T_g of the polymeric coformers.

The structural diversity and complexity of the prepared dispersions were probed by combining various experimental approaches. From the methodological point of view we found out that the relatively fast and reliable procedure allowing primary structural characterization of solid dispersions involves a combination of DSC, WAXS, ^{13}C CP/MAS NMR spectroscopy, and measurements of ^{13}C-detected $T_1(^1H)$ spin relaxation times. In this way we were able to distinguish distinct types of solid dispersions and to probe homogeneity of the systems in the scale of ca. 10−500 nm. To obtain much detail structural information, to probe the extent of intermolecular interactions, to precisely determine size of molecular clusters, and to assess the strength of H-bonding, the set of advanced ss-NMR techniques had to be applied. Hydrogen bonding was probed by ^{13}C and ^{15}N NMR experiments; ^{1}H−^{1}H and ^{1}H−^{13}C correlation experiments allowed measurements of interatomic distances and the size of molecular clusters, while ^{1}H−^{13}C WISE NMR was useful in probing segmental dynamics.

ASSOCIATED CONTENT

Supporting Information

Details of solid-state NMR experimental parameters, additional spectra and dissolution profiles, and complete relaxation data. This material is available free of charge via the Internet at http://pubs.acs.org.

AUTHOR INFORMATION

Corresponding Author

*(J.B.) E-mail: brus@imc.cas.cz.

Author Contributions

The manuscript was written through contributions of all authors. All authors have given approval to the final version of the manuscript.

Notes

The authors declare no competing financial interest.

ACKNOWLEDGMENTS

The authors gratefully acknowledge the Grant Agency of the Czech Republic for financial support (Czech Science Foundation, Grant No. P106/11/P426). The authors acknowledge the Charles University in Prague, Department of Physical and Macromolecular Chemistry, for the opportunity for the doctoral studies.

REFERENCES

(1) Sekiguchi, K.; Obi, N. Studies on absorption of eutectic mixture. I. A comparison of the behavior of eutectic mixture of sulfathiazole and that of ordinary sulfathiazole in man. *Chem. Pharm. Bull* **1961**, *9*, 866−872.

(2) Sekiguchi, K.; Obi, N.; Ueda, Y. Studies on on absorption of eutectic mixture. II. Absorption of fused conglomerates of chloramphenicol and urea in rabbits. *Chem. Pharm. Bull.* **1964**, *12*, 134−144.

(3) Mohanachandran, P. S.; Sindhumol, P. G.; Kiran, T. S. Enhancement of solubility and dissolution rate: an overview. *Pharm. Globale* **2010**, *4*, 1−10.

(4) Liu, R., Ed. *Water-Insoluble Drug Formulation*, 2nd ed.; CRC Press Taylor & Francis Group: Boca Raton, FL, 2008.

(5) Leuner, C.; Dressman, J. Improving drug solubility for oral delivery using solid dispersions. *Eur. J. Pharm. Biopharm.* **2000**, *50*, 47−60.

(6) Ghaste, R.; Dhanyakumar, C. D.; Shah, R. R.; Ghodke, D. S. Solid Dispersions: An Overview. *Pharmainfo.net* **2009**, *7* (5).

(7) Asker, A. F; Whitworth, C. W. Dissolution of acetylsalicylic acid from acetylsalicylic acid-polyethylene glycol 6000 coprecipitates. *Pharmazie* **1975**, *30*, 530−531.

(8) Bobe, K. R.; Subrahmanya, C. R.; Suresh, S.; Gaikwad, D. T.; Patil, M. D.; Khade, T. S.; Gavitre, B. B.; Kulkarni, V. S.; Gaikwad, U. T. Formulation and evaluation of solid dispersion of atorvastatin with various carriers. *Pharm. Globale* **2011**, *1*, 1−6.

(9) Caron, V.; Tajber, L.; Corrigan, O. I.; Healy, A. M. A comparison of spray drying and milling in the production of amorphous dispersions of sulfathiazole/polyvinylpyrrolidone and sulfadimidine/polyvinylpyrrolidone. *Mol. Pharmaceutics* **2011**, *8*, 532−542.

(10) Saeed, A.; Rahman, A. U.; Islam, N. U.; Saeed, M.; Ashhad Halimi, S. M. Study of interaction of drugs with body-alike macromolecule (polyvinylpyrrolidone) by ultra violet spectroscopic method. *Mal. J. Pharm. Sci.* **2006**, *4*, 63−73.

(11) Dhirendra, K.; Lewis, S.; Udupa, N.; Atin, K. Solid dispersions: A review. *Pak. J. Pharm. Sci.* **2009**, *22*, 234−246.

(12) Etrych, T.; Šírová, M.; Starovoytova, L.; Říhová, B.; Ulbrich, K. HPMA copolymer conjugates of paclitaxel and docetaxel with pH-controlled drug release. *Mol. Pharmaceutics* **2010**, *7*, 1015−1026.

(13) Kopeček, J. Biomaterials and drug delivery: Past, present, and future. *Mol. Pharmaceutics* **2010**, *7*, 922−925.
(14) Claeys, B.; Vervaeck, A.; Vervaet, C.; Remon, J. P.; Hoogenboom, R.; De Geest, B. G. Poly(2-ethyl-2-oxazoline) as matrix excipient for drug formulation by hot melt extrusion and injection molding. *Macromol. Rapid Commun.* **2012**, *33*, 1701−1707.
(15) Lindblad, B.; Persson, N. H.; Takolander, R.; Bergqvist, D. Does low-dose acetylsalicylic acid prevent stroke after carotid surgery? A double-blind, placebo-controlled randomized trial. *Stroke* **1993**, *24*, 1125−1128.
(16) Bujold, E.; Morency, A.-M.; Lacasse, Y.; Forest, J.-C.; Giguère, Y. Acetylsalicylic acid for the prevention of Preeclampsia and intrauterine growth restriction in women with abnormal uterine artery Doppler: A systematic review and meta-analysis. *J. Obstet. Gynaecol. Can. Sep.* **2009**, 818−826.
(17) Garcia-Albeniz, X.; Chan, A. T. Aspirin for the prevention of colorectal cancer. *Best Pract. Res. Clin. Gastroenterol.* **2011**, *25*, 461−472.
(18) Dressman, J. B.; Nair, A.; Abrahamsson, B.; Barends, D. M.; Groot, D. W.; Kopp, S.; Langguth, P.; Polli, J. E.; Shah, V. P.; Zimmer, M. Biowaiver monograph for immediate-release solid oral dosage forms: Acetylsalicylic acid. *J. Pharm. Sci.* **2012**, *101*, 2653−2667.
(19) Therapeutic Good Administration: Australian Public Assessment Report for Aspirin and Esomeprazole Fixed Dose Combination, PM-2010-03829-3-3 (Commonwealth of Australia, 2012).
(20) Scales, C. W.; Vasilieva, Y. A.; Convertine, A. J.; Lowe, A. B.; McCormick, C. L. Direct, controlled synthesis of the nonimmunogenic, hydrophilic polymer, poly(*N*-(2-hydroxypropyl)-methacrylamide) via RAFT in aqueous media. *Biomacromolecules* **2005**, *6*, 1846−1850.
(21) Marín, M. T.; Margarit, M. V.; Salcedo, G. E. Characterization and solubility study of solid dispersions of flunarizine and polyvinylpyrrolidone. *Farmaco* **2002**, *57*, 723−727.
(22) Bharate, S. S.; Bharate, S. B.; Bajaj, A. N. Interactions and incompatibilities of pharmaceutical excipients with active pharmaceutical ingredients: a comprehensive review. *J. Excipients Food Chem.* **2010**, *1*, 3−26.
(23) Spevacek, J.; Brus, J.; Divers, T.; Grohens, Y. Solid-state NMR study of biodegradable starch/polycaprolactone blends. *Eur. Polym. J.* **2007**, *43*, 1866−1875.
(24) Geen, H.; Titman, J. J.; Gottwald, J.; Spiess, H. W. Solid-state proton multiple-quantum NMR spectroscopy with fast magic angle spinning. *Chem. Phys. Lett.* **1994**, *227* (1−2), 79−86.
(25) Brus, J.; Urbanova, M.; Strachota, A. Epoxy networks reinforced with polyhedral oligomeric silsesquioxanes: Structure and segmental dynamics as studied by solid-state NMR. *Macromolecules* **2008**, *41*, 372−386.
(26) Salager, E.; Stein, R. S.; Steuernagel, S.; Lesage, A.; Elena, B.; Emsley, L. Enhanced sensitivity in high-resolution ^{1}H solid-state NMR spectroscopy with DUMBO dipolar decoupling under ultra-fast MAS. *Chem. Phys. Lett.* **2009**, *469*, 336−341.
(27) Schmidt-Rohr, K.; Clauss, J.; Spiess, H. W. Correlation of structure, mobility, and morphological information in heterogeneous polymer materials by 2-dimensional wideline-separation NMR-spectroscopy. *Macromolecules* **1992**, *25*, 3273−3277.
(28) Bielecki, A.; Kolbert, A. C.; Levitt, M. H. Frequency-switched pulse sequences: Homonuclear decoupling and dilute spin NMR in solids. *Chem. Phys. Lett.* **1989**, *155*, 341−346.
(29) Vinogradov, E.; Madhu, P. K.; Vega, S. High-resolution proton solid-state NMR spectroscopy by phase-modulated Lee−Goldburg experiment. *Chem. Phys. Lett.* **1999**, *314*, 443−450.
(30) van Rossum, B. J.; de Groot, C. P.; Ladizhansky, V.; Vega, S.; de Groot, H. J. M. A method for measuring heteronuclear (H-1−C-13) distances in high speed MAS NMR. *J. Am. Chem. Soc.* **2000**, *122*, 3465−3472.
(31) Proks, V.; Brus, J.; Pop-Georgievski, O.; Vecernikova, E.; Wisniewski, W.; Kotek, J.; Urbanova, M.; Rypacek, F. Thermal-induced transformation of polydopamine structures: An efficient route for the stabilization of the polydopamine surfaces. *Macromol. Chem. Phys.* **2013**, *214*, 499−507.
(32) Bielecki, A.; Burum, D. P. Temperature dependence of ^{207}Pb MAS spectra of solid lead nitrate. An accurate, sensitive thermometer for variable-temperature MAS. *J. Magn. Reson., A* **1995**, *116*, 215−220.
(33) Wilson, C. C. Interesting proton behaviour in molecular structures. Variable temperature neutron diffraction and ab initio study of acetylsalicylic acid: Characterising librational motions and comparing protons in different hydrogen bonding potentials. *New J. Chem.* **2002**, *26*, 1733−1739.
(34) Olabisi, O.; Robeson, L.; Shaw, M. *Polymer−Polymer Miscibility*; Academic Press, Inc.: San Diego, CA, 1979.
(35) Zhu, Q.; Harris, M. T.; Taylor, L. S. Time-resolved SAXS/WAXS study of the phase behavior and microstructural evolution of drug/PEG solid dispersions. *Mol. Pharmaceutics* **2011**, *8*, 932−939.
(36) Chang, C.; Díaz, L. E.; Morin, F.; Grant, D. M. Solid-state ^{13}C NMR study of drugs: Aspirin. *Magn. Reson. Chem.* **1986**, *24*, 768−771.
(37) Johansson, A.; Tegenfeldt, J. NMR study of crystalline and amorphous poly(ethylene oxide). *Macromolecules* **1992**, *25*, 4712−4715.
(38) Oh, T. J.; Nam, J. H.; Jung, Y. M. Molecular miscible blend of poly(2-cyano-1,4-phenyleneterephthalamide) and polyvinylpyrrolidone characterized by two-dimensional correlation FTIR and solid state C-13 NMR spectroscopy. *Vib. Spectrosc.* **2009**, *51*, 15−21.
(39) Goldman, M.; Shen, L. Spin−spin relaxation in LAF3. *Phys. Rev.* **1966**, *144*, 321−&.
(40) Clauss, J.; Schmidt-Rohr, K.; Spiess, H. W. Determination of domain sizes in heterogeneous polymers by solid-state NMR. *Acta Polym.* **1993**, *44*, 1−17.
(41) Caravatti, P.; Neuenschwander, P.; Ernst, R. R. Characterization of heterogeneous polymer blends by 2-dimensional proton spin diffusion spectroscopy. *Macromolecules* **1985**, *18*, 119−122.
(42) Vogt, F. G.; Yin, H.; Forcino, R. G.; Lianming, W. ^{17}O solid-state NMR as a sensitive probe of hydrogen bonding in crystalline and amorphous solid forms of diflunisal. *Mol. Pharmaceutics* **2013**, *10*, 3433−3446.
(43) Urbanova, M.; Brus, J.; Sedenkova, I.; Policianova, O.; Kobera, L. Characterization of solid polymer dispersions of active pharmaceutical ingredients by ^{19}F MAS NMR and factor analysis. *Spectrochim. Acta, Part A* **2013**, *100*, 59−66.
(44) Asano, A.; Takegoshi, K. Polymer Blends and Miscibility. In *Solid State NMR of Polymers*; Ando, I., Asakura, T., Eds.; Elsevier: New York, 1998; Chapter 10, pp 361−414.
(45) Chen, Q.; Schmidt-Rohr, K. Measurement of the local ^{1}H spin-diffusion coefficient in polymers. *Solid State Nucl. Magn.* **2006**, *29*, 142−152.
(46) Pham, T. N.; Watson, S. A.; Edwards, A. J.; Chavda, M.; Clawson, J. S.; Strohmeier, M.; Vogt, F. G. Analysis of Amorphous Solid Dispersions Using 2D Solid-State NMR and ^{1}H T_1 Relaxation Measurements. *Mol. Pharmaceutics* **2010**, *7*, 1667−1691.
(47) Schmidt-Rohr, K.; Spiess, H. W. *Multidimensional Solid-State NMR and Polymers*. Academic Press, San Diego, 1994.
(48) Nath, R.; El Goresy, T.; Geil, B.; Zimmermann, H.; Bohmer, R. Relaxation in the glass former acetylsalicylic acid studied by deuteron magnetic resonance and dielectric spectroscopy. *Phys. Rev. E* **2006**, *74* (2), 021506.
(49) Kessler, H.; Gehrke, M.; Griesinger, C. Two-dimensional NMR-spectroscopy: Background and overview of the experiments. *Angew. Chem., Int. Ed.* **1988**, *27* (4), 490−536.
(50) Li, Z. J.; Abramov, Y.; Bordner, J.; Leonard, J.; Medek, A.; Trask, A. V. Solid-state acid−base interactions in complexes of heterocyclic bases with dicarboxylic acids: Crystallography, hydrogen bond analysis, and N-15 NMR spectroscopy. *J. Am. Chem. Soc.* **2006**, *128*, 8199−8210.
(51) Harper, J. K.; Strohmeier, M.; Grant, D. M. Pursuing structure in microcrystalline solids with independent molecules in the unit cell using ^{1}H−^{13}C correlation data. *J. Magn. Reson.* **2007**, *189*, 20−31.
(52) Tatton, A. S.; Pham, T. N.; Vogt, F. G.; Iuga, D.; Edwards, A. J.; Brown, S. P. Probing hydrogen bonding in cocrystals and amorphous

dispersions using $^{14}N-^{1}H$ HMQC solid-state NMR. *Mol. Pharmaceutics* **2013**, *10*, 999−1007.
(53) Matějíček, P.; Brus, J.; Jigounov, A.; Pleštil, J.; Uchman, M.; Procházka, K.; Gradzielski, M. On the structure of polymeric composite of metallacarborane with poly(ethylene oxide). *Macromolecules* **2011**, *44*, 3847−3855.
(54) Vishweshwar, P.; McMahon, J. A.; Oliveira, M.; Peterson, M. L.; Zaworotko, M. J. The predictably elusive form II of aspirin. *J. Am. Chem. Soc.* **2005**, *127*, 16802−16803.
(55) Li, X. Y.; Wang, X.; Yu, D. G.; Ye, S.; Kuang, Q. K.; Yi, Q. W.; Yao, X. Z. Electrospun borneol−PVP nanocomposites. *J. Nanomater.* **2012**, 731382.